International Journal of Heat and Mass Transfer 156 (2020) 119869

Contents lists available at ScienceDirect

International Journal of Heat and Mass Transfer

journal homepage: www.elsevier.com/locate/hmt

Investigation of heat transfer modes in plasmonic nanoparticles

Anil Yuksel[a,*], Edward T. Yu[b], Michael Cullinan[a], Jayathi Murthy[c]

[a] Department of Mechanical Engineering, The University of Texas at Austin, Austin, Texas 78712, USA
[b] Microelectronics Research Center, Department of Electrical and Computer Engineering, The University of Texas at Austin, Austin, Texas 78758, USA
[c] Henry Samueli School of Engineering and Applied Science, University of California, Los Angeles, Los Angeles, CA 90095, USA

ARTICLE INFO

Article history:
Received 25 October 2019
Revised 24 April 2020
Accepted 24 April 2020
Available online 20 May 2020

Keywords:
Near-field thermal energy transport
Plasmonic nanoparticles
Interfacial thermal conductance

ABSTRACT

There has been much recent interest in understanding heat transfer in nanoparticle packings in nanotechnology such as emerging photonics applications. In this paper, we analyze heat transfer between two plasmonic nanoparticles in finite contact and suspended in air to delineate the dominant modes of heat transfer. We have previously investigated the heat transfer analysis of laser heating in a nanoparticle packing such that interfacial thermal conductance between the nanoparticle packings in contact and the predicted average nanoparticle packing temperature matches with the observations of laser sintering temperature well when G_{IC} is about 20 (MW/m^{2}K). When G_{IC} is less than 20 (MW/m^{2}K), the primary pathway for heat transfer is that across the particle-air-particle interface. Thermal transport in these assemblies is subject to electromagnetic field enhancements due to near-field energy transfer; however, we show that radiation heat transfer between the nanoparticles is not a significant heat transport mode. Subcontinuum thermal effects are found to strongly retard overall thermal transport between the particles through the air pathway.

1. Introduction

Nanomaterials such as nanoparticles, nanorods, nanotubes have attracted great attention in nanotechnology for a wide range of applications in optoelectronic, quantum, and photonic devices and systems, as they have unique thermal and optical properties which are quite different from their bulk properties, which can be tuned by controlling their composition, shape, and size [1,2]. Plasmon resonances can occur in a material when the material's frequency-dependent complex dielectric function approaches the negative of that for the surrounding dielectric medium [3,4]. Metal nanoparticles have been most extensively explored in these plasmonic applications due to their high electron concentrations, leading to plasmon resonances at or near visible wavelengths. In addition, coherent conduction-band collective electron oscillations in metal nanoparticles can support localized and surface plasmon polaritons (SPPs) [3,5]. These oscillations can result in enormous electromagnetic field enhancements at metal-dielectric interfaces which lead to intense scattering and absorption of light at the resonance of the optical excitation [5,6]. Collective plasmon oscillations are influenced by the structure and geometry of the nanoparticles, and local enhancements in near-field intensity between nanoparticles arranged in clusters can become especially high [7,8].

Nanofluids in which nanoparticles are in a dilute suspension have been of growing interest, as metal nanoparticles can be prevented from oxidization and agglomeration as well as exhibiting potentially enhanced optical and thermal properties [9–11]. Laser illumination and heating of nanoparticles that are in a surrounding fluid medium is of increasing interest in nanotechnology such as photonic sintering for electronics, and in photothermal applications [12–15]. High intensity laser radiation can change the properties of both the condensed matter particles and the surrounding effective medium [14,15]. Thus, analysis of nanoscale plasmonic heating in nanoparticle assemblies and from nanoparticles to a fluid environment has become crucial to the creation and understanding of the near-field thermal energy transport around nanoparticles. However, there are many challenges in understanding heat transfer at the sub-micron scale because the characteristic mean free path of the heat carriers becomes comparable to the characteristic dimensions of the nanoparticles. For example, ballistic conditions can dominate both phonon and electron transport when electrons are moving across small distances, resulting in nonequilibrium thermal conditions between the energy carriers, which becomes significant at picosecond (10^{-12} s) time scales [16,17]. Thus, electron and lattice temperatures must be analyzed individually when laser pulse durations are shorter than the effective time required for lattice and electron temperatures to equilibrate. Due

* Corresponding author.
E-mail address: anil.yuksel@utexas.edu (A. Yuksel).

https://doi.org/10.1016/j.ijheatmasstransfer.2020.119869
0017-9310/

to this non-equilibrium thermal process, the lattice temperature could be lower than the electron temperature [16–18]. Specifically, laser energy is absorbed initially by the conduction electrons in metal nanoparticles via photon-electron interactions. The electron Fermi distribution is reestablished during the electron relaxation time, which is on the order of femtoseconds (10^{-15} sec) [19,20]. Heat transport to the lattice via electron-phonon interactions occurs at a later stage, with the electron-phonon coupling time being on the order of tens of picoseconds. Collisions of electrons with the other electrons, lattice defects, and boundaries results in heating of metal nanoparticles; and energy exchange and the increase in the lattice temperature of metal nanoparticles are determined by the efficiency of these collisions. Since thermalization time, which is the characteristic time for electrons and lattice to reach thermal equilibrium, and the laser pulse width are often comparable, a two-step temperature model has been widely used to describe this thermal energy transfer [21,22].

The diffusion equation can still be used to analyze the energy transfer if the applied laser pulse width is much longer than the electron-lattice and electron-photon relaxation times [23,24]. Heat dissipation from the metal nanoparticles to the surrounding medium occurs at a longer timescale [25] so understanding the effect of this excess heat transfer on the surrounding medium and the influence of plasmonic interactions between the nanoparticles become essential. Moreover, reductions in electron mean free path due to interfacial or boundary scattering and electron-electron scattering lead to thermalization of the electron gas at the elevated temperature [26] near the metal nanoparticles and the surrounding medium, and it becomes very important to understand the effect of this on overall plasmonic heating.

Interfacial thermal conductance, or Kapitza conductance, between the nanoparticles and the surrounding medium results in a finite temperature discontinuity across the interface [27,28]. The interface's resistance to thermal flow becomes very important and plays a key role in the effective thermal resistance between the nanoparticle and the surrounding medium. Thus, sub-micron heat transfer effects also need to be considered when the characteristic length scale of energy carriers becomes comparable to the diameter of the nanoparticles. Whether these effects are important depends on the thermal resistance of competing pathways in the system. For two nanoparticles in contact, for example, heat conduction through the particle volume occurs in series with heat transfer across the contact resistance between particles. This interfacial thermal conductance is dependent not only on the material properties of the two particles, but also on the interfacial roughness, effective contact area, contact pressure, and other factors [28–30]. In addition, radiation heat transfer between particles, including near-field radiative transport, as well as conduction heat transfer through the air or other medium surrounding the particles, may also play a role [31,32].

In this paper, we consider a situation commonly encountered in many laser-induced plasmonic heating applications such as packing of metallic nanoparticles irradiated by a laser for a duration far longer than the relaxation time of carriers within the system. We conduct a scale analysis to evaluate the competing pathways for heat transfer within the particle assembly, and identify interfacial contact conductance as an important factor controlling heat transfer in the assembly. We also analyze the dominant modes of heat transfer in a metal nanoparticle assembly which are irradiated by laser, and validate the model by comparing the predicted average nanoparticle packing temperature with experimental data.

2. Nanoscale thermal model

We developed an electromagnetic-thermal model to estimate the temperature distribution of copper nanoparticle packings that have a log-normal distribution with 116 nm mean nanoparticle radius and 48 nm standard deviation which corresponds to values measured experimentally. Agglomeration was prevented within the nanoparticles by applying coating on their surface and nanoparticles were suspended in ink solution that result in having not finite contact area between the nanoparticles. In other words, nanoparticles were closely spaced and having minimal contact with each other. The effect of cohesive forces between the particles that create the particle packing was initially simulated by DEM [9], which was used as a geometry input for the electromagnetic-thermal model. Very good observation was made between the DEM results and the experimentally investigated nanoparticle distribution from our previous work [33]. The optical interactions due to the electromagnetic heating in the coupled model were analyzed by calculating the energy absorption efficiency of the randomly distributed nanoparticles packings [34], and a volumetric heat source due to laser-particle interactions was included in the thermal computations [33] under various laser fluences which the laser deposition time is much larger than carrier relaxation times. A heat transfer model was then implemented to simulate the thermal interactions within the nanoparticle packing. A Finite Element Analysis (FEA) was applied to solve the coupled electromagnetic-heat transfer model numerically by implementing an interfacial thermal resistance at the surface of each nanoparticle interface as a boundary condition in COMSOL [35]. We varied the value of the interfacial thermal conductance G_{IC} in the model to fit experimental results indicating that sintering of copper nanoparticles starts around 700 K [33]. It was observed that the mean nanoparticle packing temperature reaches 730 K when G_{IC}=20 (MW/m^{2}K) under a laser irradiation of 2.6 kW/cm^2 in the electromagnetic-thermal model, which is close to the temperature observed in experiments with similar laser illumination powers [33]. Additional details regarding this model can be found in Ref. [33].

As depending on the deposition and the nanomanufacturing technique, the contact area between the nanoparticles could be different which is also very difficult to measure at nanoscale. Thus, we further elucidate the results from our previous work by using the parameters identified as most important in influencing heat transfer and analyzing the influence of variations in those parameters on thermal transport in a model two-particle assembly in the present work. Specifically, we use a typical two nanoparticle assembly in which two nanoparticles that are 100 nm radius and with a finite contact by varying the contact radius from 2 to 8 nm -based on our numerical and experimental observations from our previous work [33]- to analyze the heat transfer modes between the nanoparticles in detail. Moreover, the effect of thermal transport between the two nanoparticles that are 100 nm radius were compared with the other particle sizes that are mainly observed from the log-normal distribution of nanoparticle packing with 116 nm mean nanoparticle radius and 48 nm standard deviation when two nanoparticle assembly are in finite contact.

We consider heat transfer between two identical copper nanoparticles in contact, surrounded by air, as shown in Fig. 1. The distance and the contact radius between the two nanoparticles are also labelled as ($l_{1,2}$) and (R_c), respectively. There are three main modes of heat transfer between the two nanoparticles: (1) thermal conduction between the particles ($G_{overall\,conduction}$), which consists of thermal conduction through the constriction at the contact ($G_{contact}$), and thermal conduction across the interface between them ($G_{particle}$), (2) thermal conduction through the air surrounding the particles (G_{air}), and (3) thermal radiation between the particles (G_{rad}). These modes of heat transfer are illustrated in Fig. 1 and represented by the circuit diagram in Fig. 2. Thermal modeling parameters used in the nanoscale thermal model in this study is also provided in Table 1.

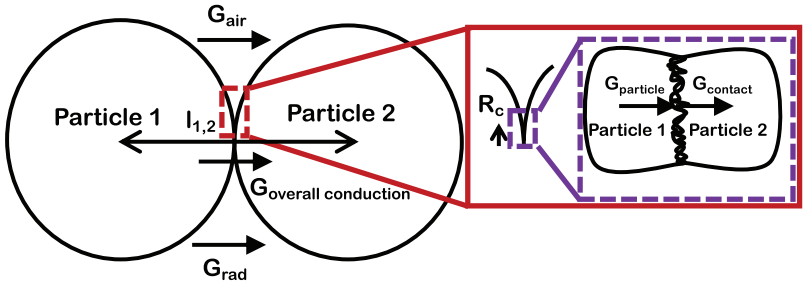

Fig. 1. Heat transfer modes between contacting particles.

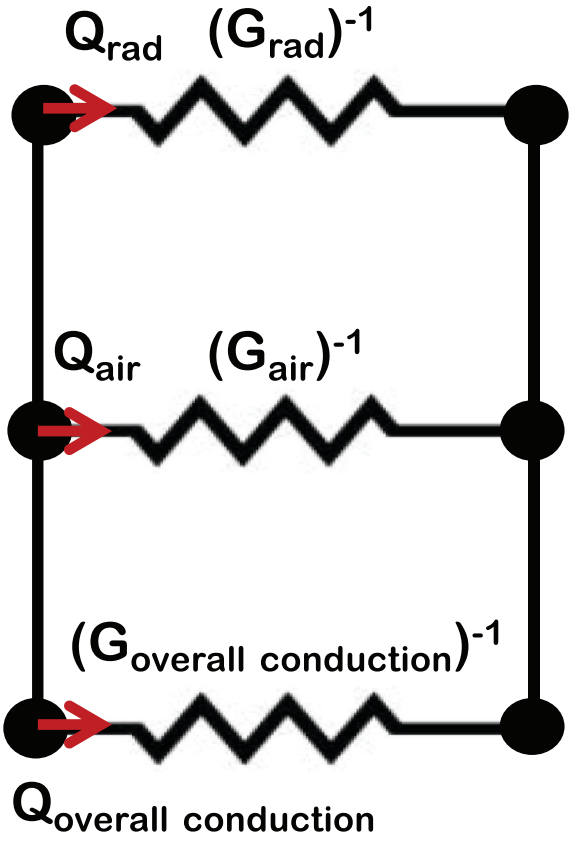

Fig. 2. Schematic of heat transfer resistance between the particles.

Table 1
Thermal modeling parameters.

Parameter	Value
Particle Radius (R_1, R_2)	100 nm
Effective Thermal Conductivity of 100 nm Particles(k_1, k_2)	330 W/mK
Bulk Thermal Conductivity of Air at 700 K(k_{air})	0.052 W/mK
Radius of Contact Area (R_c)	2 nm-8 nm
Particle's Temperature (T_1, T_2)	701 K and 700 K

2.1. Thermal conduction through constriction between particles

Thermal conduction occurs between the two contacting particles through the constriction between them, as illustrated in Fig. 1. In the diffusive limit, the total heat transfer rate between the two particles is given by Eq. (1) [36]:

$$Q_r^{(1,2)} = \frac{4k_1k_2}{(k_1+k_2)} R_c(T_1 - T_2) \tag{1}$$

where k is the thermal conductivity, $l_{1,2}$ is the distance between the centers of the two particles, R_1 and R_2 are the radii of particles 1 and 2, and R_c is the radius of the contact area [37]:

$$R_c = \sqrt{R_1^2 - \left(\frac{R_1^2 - R_2^2 + l_{1,2}^2}{2l_{1,2}}\right)^2} \tag{2}$$

Therefore, the diffusive thermal constriction conductance for two identical particles in W/K is given by

$$G_{particle,d} = 2k_1R_c \tag{3}$$

Prasher [38] and Singh et al. [39] analyzed heat transfer for the situation when the length scale of the contact is of the same order or smaller than the mean free path of carriers. For metallic nanoparticles, electron mean free paths are of the order 10–100 nm, and depending on the length scale of the contact, ballistic constriction effects may be important. The ballistic conductance is given by [38]:

$$G_{particle,b} = \frac{6\pi k_1 R_c}{8Kn} \tag{4a}$$

where the Knudsen number Kn ($=\lambda/R_c$), and λ is the mean free path of electrons in the metal. Following [38], an estimate of the constriction conductance for Knudsen numbers ranging from diffusive to ballistic may be found by adding the ballistic and diffusive resistances. The corresponding constriction conductance is given by

$$G_{particle} = \frac{2k_1R_c}{\left(1 + \frac{8Kn}{3\pi}\right)} \tag{4b}$$

2.2. Interfacial thermal conductance between particles

Interfacial thermal conductance due to closely spaced plasmonic nanoparticles is critical for understanding the thermal transport between particles. There are various interfacial and surface irregularity effects which may create high resistance to thermal transport [40]. In order to estimate the likely range of the interfacial thermal conductance, G_{IC}, we employed an electromagnetic-thermal model described in our previous work and it is observed that at G_{IC}=20 (MW/m^{2}K), the mean nanoparticle packing temperature matches very well with the experimental results [33,34]. Hence, G_{IC}=20 (MW/m^{2}K) is used for the analysis in this work, except when otherwise indicated. The experiments employ a few-nanometer thick dielectric coating on the nanoparticles in order to prevent oxidization and corrosion [41,42]. This is expected to increase the thermal resistance, and is effectively absorbed into the value of G_{IC} in our simulations and analysis.

Cahill et al. [43] studied thermal conductance values for a variety of interfaces and found them to fall approximately in the range 10–100 (MW/m^{2}K). However, there is no published experimental work specifically addressing interfacial thermal conductance between plasmonic nanoparticles to our knowledge.

The contact conductance $G_{contact}$ is evaluated as in Eq. (5) where A_C is the finite contact area defined as $\pi {R_C}^2$.

$$G_{contact} = G_{IC}A_C \tag{5}$$

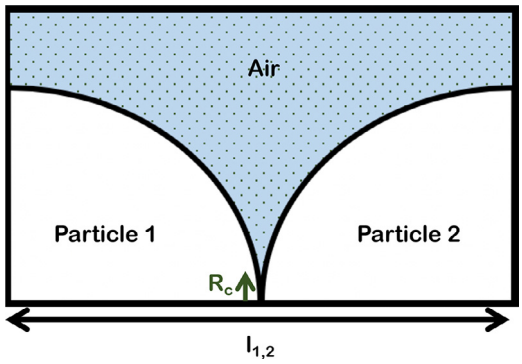

Fig. 3. The geometrical model used in numerical analysis to calculate thermal transport across particle-air-particle system.

2.3. Thermal conduction between the particles through the air

Heat transfer due to thermal conduction through the air between the particles may be significant when two particles are close together or in contact [44] as the mean free path of air could potentially have an impact on the finite temperature jump at the particle-air boundaries. So, the heat transfer between the particle (Q_{pa}) and the surrounded gas medium (air) in the sub-continuum regime is calculated by solving the diffusion equation in the air medium by applying the temperature slip boundary condition on the nanoparticle surfaces [39] for two nanoparticle assembly. Fig. 3 illustrates the two nanoparticle assembly's computational domain in which 3D-Finite Element Method (FEM) is applied to find Q_{pa} by solving Eq. (6) where k_{eff} is the effective thermal conductivity of the air. Temperature slip boundary condition as shown in Eq. (7) is used on the nanoparticle surfaces such that nanoparticle's surface temperature ($T_{nanoparticle\,surface}$) is kept at 701 K and 700 K, respectively. Convective heat flux boundary condition can be expressed on the nanoparticle surfaces as $(-n \cdot q = h_{eff}(T_{slip|\ boundary} - T_{nanoparticle\ surface}))$ shown in Eq. (8a). Thus, effective convective heat coefficient (h_{eff}) can be written as a function of k_{eff} and a constant (A) shown in Eq. (8b). A has a function of accommodation coefficient of air molecules on the nanoparticle surface (α_{air}) which is ≈ 0.9 [17], specific heat ratio (η), dynamic viscosity of air (ν) and Prandtl number (Pr). All other boundaries are also chosen as insulated.

$$k_{eff}\nabla^2 T = 0 \tag{6}$$

$$T_{slip|\ boundary} = T_{nanoparticle\ surface} + A\frac{\partial T}{\partial n} \tag{7}$$

$$\frac{\partial T}{\partial n} = \frac{k_{eff}}{A}\left(T_{slip|\ boundary} - T_{nanoparticle\ surface}\right) \tag{8a}$$

$$A = \frac{2-\alpha_{air}}{\alpha_{air}}\frac{2\eta}{\eta+1}\frac{2\nu}{Pr}\sqrt{\frac{\pi}{8RT}} \tag{8b}$$

The mean free path of gas molecules in air at atmospheric pressure and a temperature of 300 K is 66.5 nm [17] and scales as $\sqrt{T}$; at the sintering temperature of 700 K, the mean free path would be about 104 nm [39]. Thus, the Knudsen number Kn $(=\lambda/R_c)$ for thermal transport in air becomes approximately 1–1.5 and a reduction in bulk thermal conductivity of air (k_{air}) is expected because of boundary scattering and sub-continuum effects that yields a reduction in gas-phase mean free path.

Singh et al. [39] computed heat transfer for a spherical particle on a substrate in air, considering phonon transport in the particle and substrate and gas phase transport in the air. The phonon Boltzmann transport equation (BTE) was solved in the sphere, and the heat diffusion equation in the air, by applying temperature slip boundary conditions between the sphere and air. They found that gas pathway may be significant for smaller contact areas and lower particle conductivities than those considered here. Singh et al. [39] extended this framework by considering the coupled transport of phonons and gas molecules through a single integrated BTE for both carriers.

An estimate of the potential impact of sub-continuum heat transfer in the gas phase may be found by considering heat transfer in a plane layer of air bounded by walls at different temperatures. We may estimate the reduction in thermal conductivity [17] in the Knudsen number range of interest as

$$\frac{k_{eff}}{k_{\text{air}}} = \left(1 + Kn\frac{2-\alpha_T}{\alpha_T}\frac{9\gamma-5}{\gamma+1}\right)^{-1} \tag{9}$$

Here α_{T} is the thermal accommodation coefficient and γ is the specific heat ratio of air. Using the above expression, $\frac{k_{eff}}{k_{air}}$ can be estimated to be in the range 0.15–0.21 for α_T=0.9 [39]. Thus, a significant reduction in thermal conductivity of air may be expected at these length scales and operating conditions. Thus, the thermal conduction conductance (G_{air}) through the air between the particles in W/K can be found by Eq. (10), where ΔT is the temperature difference between the nanoparticles which is kept by 1 K.

$$G_{air} = \left(\frac{Q_{pa}}{\Delta T}\right) \tag{10}$$

2.4. Near-field thermal radiation between the particles

Near-field thermal radiation heat transfer between two particles may be represented by Eq. (11)

$$G(\omega,\ T, d) = \pi dRh_{\omega}(d) \tag{11}$$

where d is the gap between the particles and $h_{\omega}(d)$ is the near-field heat transfer coefficient [17]. The near-field heat transfer coefficient can be expressed by Eq. (12) which represents the contribution of surface polaritons in the near-field. Here ϵ_1 and ϵ_2 are the dielectric functions of the particles 1 and 2, respectively, $k_B$is Boltzmann's constant, and $2\pi\hbar$ is Planck's constant.

$$h_{\omega}(d) = \frac{1}{\pi^2 d^2}\frac{\epsilon''_1\epsilon''_2}{|1+\epsilon_1|^2|1+\epsilon_2|^2}k_B\left(\frac{\hbar\omega}{k_BT}\right)^2\frac{\exp\left(\frac{\hbar\omega}{k_BT}\right)}{\left(\exp\left(\frac{\hbar\omega}{k_BT}\right)-1\right)^2} \tag{12}$$

Hence, the thermal conductivity due to near field radiation (G_{rad}) is given by Eq. (13).

$$G_{rad} = \int_0^{\infty} G(\omega,\ T, d)d\omega \tag{13}$$

3. Overall heat transfer analysis

In this section, we investigate the heat transfer between two copper nanoparticles with radii of 100 nm each. The average temperature of nanoparticles is set to be about 700 K which is the approximate temperature at which sintering is observed to start. The nanoparticles are all assumed to have diffuse surfaces and are treated as completely opaque. The contact radius (R_c) between the nanoparticles is observed to be between 2 nm-8 nm in our nanoparticle packing simulations [33]. The overall conduction due to constriction resistance and interfacial contact resistance is a series combination of the two resistances so the overall conduction conductance ($G_{overall\,conduction}$) can be expressed as in Eq. (14). As the air resistance and the radiation resistances are parallel pathways with the pathways through the particles, total conductance

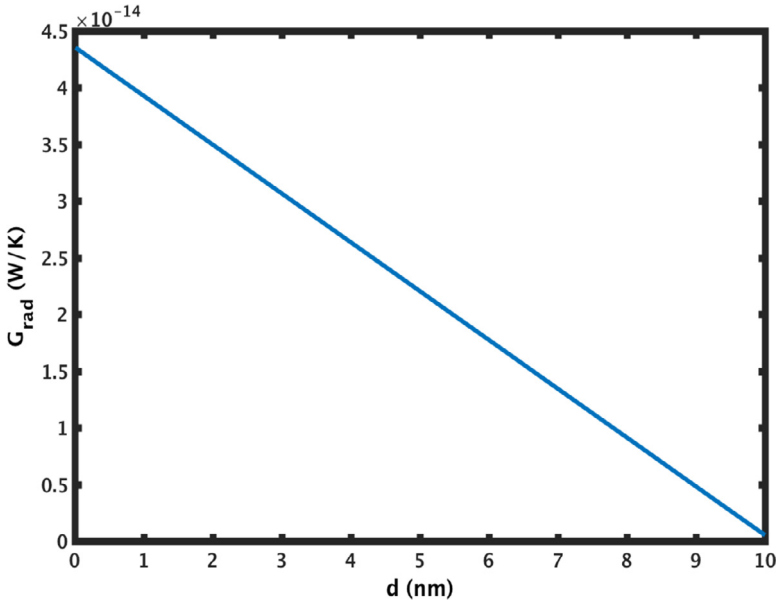

Fig. 4. G_{rad} vs. distance between the particles (d).

(G_{total}) can be calculated by Eq. (15).

$$G_{overall\ conduction} = \frac{G_{particle} \times G_{contact}}{G_{particle} + G_{contact}} \tag{14}$$

$$G_{total} = G_{overall\ conduction} + G_{air} + G_{rad} \tag{15}$$

For a 100 nm radius copper nanoparticle with contact radius R_c in the range of 2 nm - 8 nm, $G_{particle}$ is computed to be approximately 2.9 × 10^{-8} – 4.4 × 10^{-7} W/K. For this range contact radii, $G_{contact}$ is approximately 2.5 × 10^{-10} – 4 × 10^{-9} W/K given G_{IC} = 20 MW/m^{2}K from our earlier study [33]. Thus, it is clear that $G_{contact}$ is the controlling parameter in determining $G_{overall\ conduction}$ for the range of parameters involved. Ballistic carrier transport effects are important in determining the constriction resistance; however, heat transfer through the contact is controlled almost entirely by the interfacial contact resistance.

For the example of two particle system, the conductance through the air between the particles (G_{air}) is found as approximately 4.5 × 10^{-10} W/K assuming effective thermal conductivity for air; this is comparable with conduction through the contact ($G_{contact}$) when R_c is 2 nm and G_{air} starts to reduce by up to an order of magnitude smaller than $G_{contact}$ when R_c is 8 nm. Thus, it is found that the conduction through the air surrounding the particles will only start to become important when G_{IC} is less than ~3 MW/m^{2}K when gas (air) rarefaction effects is considered. Heat transfer due to radiation is also calculated to be at least four orders-of-magnitude lower than the heat transfer due to conduction between the particles (G_{rad} = ~4.4 × 10^{-14} W/K at 730 K for a particle separation distance of 0.01 nm and illustrated in Fig. 4 as a function of distance). Therefore, the radiative heat transfer between particles is not a significant effect in the overall heat transfer between the particles, which is consistent with literature [45].

Overall, this exemplar two particle system shows that the most significant mode of heat transfer between the particles in the nanoparticle cluster is particle-to-particle conduction through the contact interface between the particles and that the overall thermal conductivity of the nanoparticle cluster is set by the interfacial contact conductance, G_{IC}. However, this result is dependent on the exact contact radius, particle radius, and interfacial contact resistance of the particles. For example, more heat transfer through the air between the particles will occur if the particle size increases and everything else is held constant. Similarly, if the contact radius (R_c) decreases with all the other parameters held constant, the proportion of the heat transfer through the air will increase relative the other heat transfer modes. The effect of the contact radius on the mode of heat transfer is shown in Fig. 5. When R_c is less than 3 nm, G_{air} becomes an important mode of heat transfer for the 100 nm particle system with an interfacial contact conductance of 20 MW/m^{2}K.

As the exact contact area is difficult to estimate between the nanoparticles, the effect of the contact areas is characterized typically by a Hertzian contact model based on the particle-to-particle interactions once the particles are allowed to settle into their final, lowest energy configuration [9]. This means that particle sizes, solvent medium properties, and particle coating determine the exact contact areas between the particles. Thus, exact contact area is expected to vary from particle to particle and from nanoparticle cluster to cluster as they would be in typical experimental nanoparticle packings. Therefore, the uncertainty of the exact particle size is already captured in the uncertainty analysis presented in our previous work [9,33,46,47] and the effect of contact area is investigated in this work to understand the thermal transport between the most common particle sizes within the experimentally observed particle distribution. However, the interfacial contact conductance is an estimate designed to match average particle packing temperature with measured experimental data [33]. Further research is necessary in order to determine this value more precisely.

4. Effect of interfacial thermal conductance on overall heat transfer modes

The effect of the thermal interface conductance on the ratio of the heat transfer through the air to the heat transfer through the particle-to-particle interface for contact radius of R_c=8 nm was calculated and is presented in Fig. 6. For interfacial conductance constants less than 20 MW/m^{2}K, the effect of thermal conduction through the air (G_{air}) becomes very important and the dominant mode of the heat transfer happens to be not interfacial contact conductance. Therefore, G_{air} starts to become significant as both

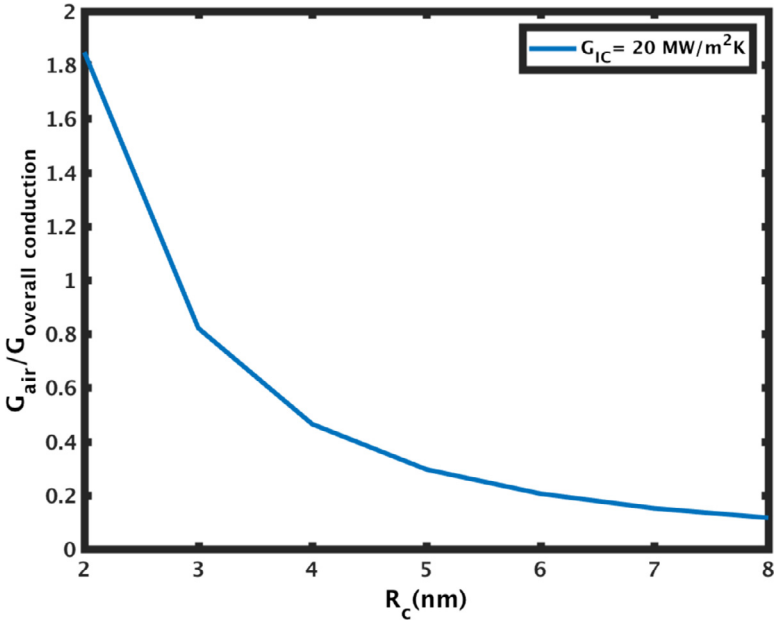

Fig. 5. $G_{air}/G_{overall\ conduction}$ vs. R_c.

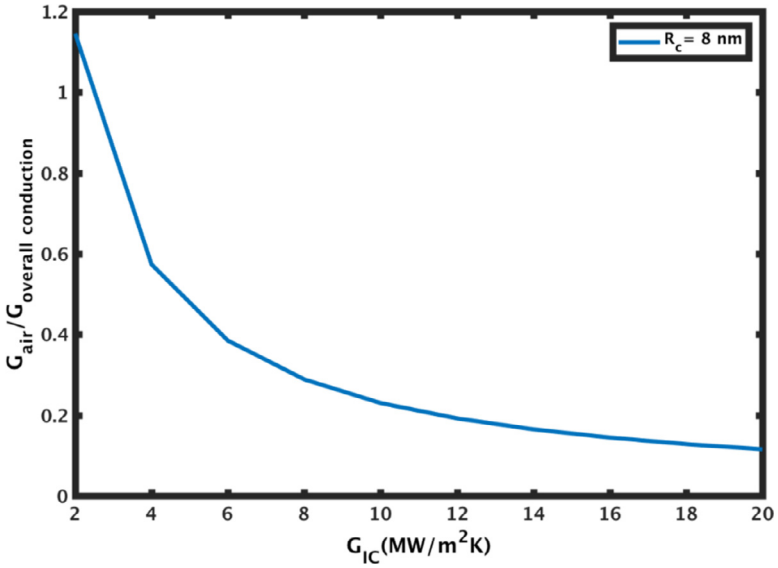

Fig. 6. $G_{air}/G_{overall\ conduction}$ vs. G_{IC} for R_c =8 nm.

interface and air conductance are important modes of heat transfer.

Since the preliminary analysis of the two particle system shows that the exact value of G_{IC} can have a significant effect on the heat transfer modes, a study was conducted to determine the effect of the interfacial thermal conductance constant on the average temperature in the nanoparticle packing based on our previous study [33]. The results of this study, shown in Fig. 6, suggest that when G_{IC} is less than 20 MW/(m^{2}K) for R_c=8 nm such that $G_{contact}$ becomes approximately as 4×10^{-9} W/K, the nanoparticles' temperature are expected to be highly dependent on the G_{IC} value. Once G_{IC} is less than about 3 MW/(m^{2}K), conduction through the air around the nanoparticle controls the overall mode of heat transfer. This makes sense because as G_{IC} decreases more of the heat transfer occurs through the air as opposed to through the interface between the particles. Also, nanoparticles' temperature are expected to decrease very gradually with increase of G_{IC} beyond 20 MW/(m^{2}K).

The calculated G_{air} for two 100 nm particle radius is also compared with most commonly observed different radius of particle sizes (R_1, R_2) within the previously analyzed nanoparticle packing distribution [33]. As the G_{air} is calculated from the FEM simulation described in Section 2.3, the R_c is automatically scaled with the analyzed particle sizes shown in Table 2. It is observed that as the particle size difference increases, G_{air} starts to increase. For instance, for case 5 that represents the 180 nm radius particles, G_{air} is found more than 3 times of the 100 nm radius two nanoparticle assembly case. This ratio $(G_{air}(R_1/R_2)/G_{air}(100\,\text{nm}/100\,\text{nm}))$ further increases with increasing particle size and becomes more than 11 times when particle radius becomes 374 nm. This makes sense because surface area that thermal transport happens between particle-air increases which leads to enhancing the contribution of

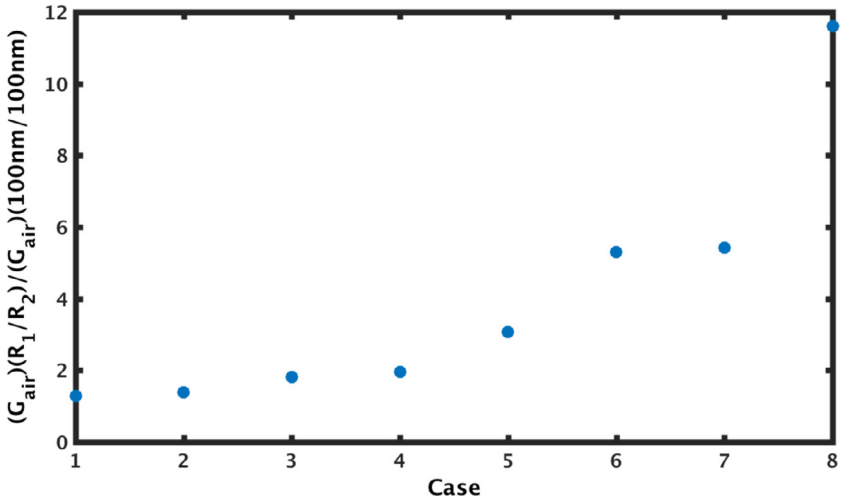

Fig. 7. $G_{air}(R_1/R_2)/G_{air}(100\,\text{nm}/100\,\text{nm})$ vs. Case.

Table 2
Effect of particle size on thermal conduction through air.

Case	(R_1, R_2)	$(G_{air})(R_1/R_2)/(G_{air})(100\text{ nm}/100\text{ nm})$
1	(181 nm, 100 nm)	1.29
2	(245 nm, 100 nm)	1.39
3	(310 nm, 100 nm)	1.81
4	(374 nm, 100 nm)	1.96
5	(180 nm, 180 nm)	3.06
6	(245 nm, 310 nm)	5.31
7	(245 nm, 245 nm)	5.43
8	(374 nm, 374 nm)	11.61

G_{air} onto the overall heat transfer modes. All cases compared with the two particle (100 nm, 100 nm) case is also illustrated in Fig. 7.

However, these large temperature gradients between particles have typically not been observed in our experiments as evidenced by the good uniformity in the sintering of the nanoparticles within sintering spot even when the laser power is near the sintering threshold [48,49]. If there were large temperature gradients between particles, we would expect to see some particles that are above the sintering threshold temperature start to neck and sinter before the other particles that are at lower temperatures. Further studies are needed for the effect of the morphological change on overall heat transfer modes during the transient laser heating.

5. Conclusion

The mechanisms of thermal transport between the plasmonic nanoparticles suspended in air were investigated in this study. It was observed that the overall heat conduction is dominated by the contact resistance between the nanoparticles. Furthermore, radiation is not an important mode of heat transfer and is at least five orders of magnitude lower than the heat transfer due to conduction between the particles. When $G_{lC} < 20$ (MW/m^{2}K), conduction heat transfer from the plasmonic nanoparticles to the air was observed to be important due to the nanoscale thermal effects. Particle size and contact radius were observed to affect the contribution of the heat transfer modes; thus, the structure of the two plasmonic nanoparticle in contact and suspended in air under laser heating could change the dominant mode of overall heat transfer. This could provide insight into designing novel nanoparticle self-assemblies to enhance the thermal transport between the plasmonic nanoparticles.

Declaration of Competing Interest

The authors declare that they have no known competing financial interests or personal relationships that could have appeared to influence the work reported in this paper.

Supplementary materials

Supplementary material associated with this article can be found, in the online version, at doi:10.1016/j.ijheatmasstransfer.2020.119869.

CRediT authorship contribution statement

Anil Yuksel: Conceptualization, Methodology, Validation, Investigation, Writing - review & editing. **Edward T. Yu:** Supervision, Writing - review & editing. **Michael Cullinan:** Supervision, Resources. **Jayathi Murthy:** Supervision, Writing - review & editing, Investigation.

References

[1] I.O. Sosa, C. Noguez, R.G. Barrera, Optical properties of metal nanoparticles with arbitrary shapes, J. Phys. Chem. B 107 (26) (2003) 6269–6275.
[2] ... M. Hu, J. Chen, Z.Y. Li, L. Au, G.V. Hartland, X. Li, Y. Xia, Gold nanostructures: engineering their plasmonic properties for biomedical applications, Chem. Soc. Rev. 35 (11) (2006) 1084–1094.
[3] , Near-field Optics and Surface Plasmon Polaritons, 81, in: S. Kawata, M. Ohtsu, M. Irie (Eds.), Springer Science & Business Media, 2001.
[4] F. Wang, Y.R. Shen, General properties of local plasmons in metal nanostructures, Phys. Rev. Lett. 97 (20) (2006) 206806.
[5] S.A. Maier, H.A. Atwater, Plasmonics: localization and guiding of electromagnetic energy in metal/dielectric structures, J. Appl. Phys. 98 (1) (2005) 10.
[6] A.V. Zayats, I.I. Smolyaninov, Near-field photonics: surface plasmon polaritons and localized surface plasmons, J. Opt. A. 5 (4) (2003) S16.
[7] S.A. Maier, P.G. Kik, H.A. Atwater, Observation of coupled plasmon-polariton modes in Au nanoparticle chain waveguides of different lengths: estimation of waveguide loss, Appl. Phys. Lett. 81 (9) (2002) 1714–1716.
[8] B. Luk'yanchuk, N.I. Zheludev, S.A. Maier, N.J. Halas, P. Nordlander, H. Giessen, C.T. Chong, The Fano resonance in plasmonic nanostructures and metamaterials, Nat. Mater. 9 (9) (2010) 707.
[9] A. Yuksel, M. Cullinan, Modeling of nanoparticle agglomeration and powder bed formation in microscale selective laser sintering systems, Add. Manufact. 12 (2016) 204–215.
[10] M.M. Miller, A.A. Lazarides, Sensitivity of metal nanoparticle surface plasmon resonance to the dielectric environment, J. Phys. Chem. B 109 (46) (2005) 21556–21565.
[11] A. Yuksel, M. Cullinan, E.T. Yu, J. Murthy, Enhanced plasmonic behavior of metal nanoparticles surrounded with dielectric shell, ASME 2019 International Mechanical Engineering Congress and Exposition, American Society of Mechanical Engineers Digital Collection, 2019.

[12] P. Keblinski, D.G. Cahill, A. Bodapati, C.R. Sullivan, T.A. Taton, Limits of localized heating by electromagnetically excited nanoparticles, J. Appl. Phys. 100 (5) (2006) 054305.
[13] P.V. Kazakevich, A.V. Simakin, V.V. Voronov, G.A. Shafeev, Laser induced synthesis of nanoparticles in liquids, Appl. Surf. Sci. 252 (13) (2006) 4373–4380.
[14] X. Huang, P.K. Jain, I.H. El-Sayed, M.A. El-Sayed, Plasmonic photothermal therapy (PPTT) using gold nanoparticles, Laser. Med. Sci. 23 (3) (2008) 217.
[15] M. Honda, Y. Saito, N.I. Smith, K. Fujita, S. Kawata, Nanoscale heating of laser irradiated single gold nanoparticles in liquid, Opt. Express 19 (13) (2011) 12375–12383.
[16] G. Chen, Nanoscale Energy Transport and conversion: a Parallel Treatment of electrons, molecules, phonons, and Photons, Oxford University Press, 2005.
[17] Z.M. Zhang, Nano/microscale Heat Transfer, 2007 (No. Sirsi) i9780071436748).
[18] T.Q. Qiu, C.L. Tien, "Femtosecond laser heating of multi-layermetals-I analysis, Int. J. Heat Mass Transfer 37 (1994) 2789–2797.
[19] R.H. Groeneveld, R. Sprik, A. Lagendijk, Femtosecond spectroscopy of electron–electron and electron-phonon energy relaxation in Ag and Au, Phys, Rev. B 51 (17) (1995) 11433.
[20] D.Y. Tzou, J.K. Chen, J.E. Beraun, "Hot-electron blast inducedby ultrashort--pulsed lasers in layered media, Int. J. Heat Mass Transfer 45 (2002) 3369–3382.
[21] L. Jiang, H.L. Tsai, Improved two-temperature model and its application in ultrashort laser heating of metal films, J. Heat Transf. 127 (10) (2005) 1167–1173.
[22] J.K. Chen, D.Y. Tzou, J.E. Beraun, A semiclassical two-temperature model for ultrafast laser heating, Int. J. Heat Mass Transf. 49 (1–2) (2006) 307–316.
[23] B. Rethfeld, A. Kaiser, M. Vicanek, G. Simon, "Ultrafast dynam-ics of nonequilibrium electrons in metals under femtosecond laser irradia-tion, Phys. Rev. B 65 (2002) 214303–214313.
[24] C.P. Grigoropoulos, Transport in Laser Microfabrication: Fundamentals and Applications, Cambridge University Press, 2009.
[25] E.L. Keller, N.C. Brandt, A.A. Cassabaum, R.R. Frontiera, Ultrafast surface-enhanced Raman spectroscopy, Analyst 140 (2015) 4922–4931 https://doi.org/10.1039/c5an00869g.
[26] S. Linic, U. Aslam, C. Boerigter, M. Morabito, Photochemical transformations on plasmonic metal nanoparticles, Nat. Mater. 14 (2015) 567–576 https://doi.org/10.1038/nmat4281.
[27] W. Evans, R. Prasher, J. Fish, P. Meakin, P. Phelan, P. Keblinski, Effect of aggregation and interfacial thermal resistance on thermal conductivity of nanocomposites and colloidal nanofluids, Int. J. Heat Mass Transf. 51 (5–6) (2008) 1431–1438.
[28] J.L. Barrat, F. Chiaruttini, Kapitza resistance at the liquid—solid interface, Mol. Phys. 101 (11) (2003) 1605–1610.
[29] G.L. Pollack, Kapitza resistance, Rev. Mod. Phys. 41 (1) (1969) 48.
[30] E.T. Swartz, R.O. Pohl, Thermal boundary resistance, Rev. Mod. Phys. 61 (3) (1989) 605.
[31] J.A. Eastman, S.R. Phillpot, S.U.S. Choi, P. Keblinski, Thermal transport in nanofluids, Annu. Rev. Mater. Res. 34 (2004) 219–246.
[32] P. Keblinski, J.A. Eastman, D.G. Cahill, Nanofluids for thermal transport, Mater. Today 8 (6) (2005) 36–44.
[33] A. Yuksel, E.T. Yu, M. Cullinan, J. Murthy, Thermal transport in nanoparticle packings under laser irradiation, J. Heat Transf. 142 (3) (2020).
[34] A. Yuksel, T.Y. Edward, M. Cullinan, J. Murthy, Effect of particle size distribution on near-field thermal energy transfer within the nanoparticle packings, J. Photon. Energy 9 (3) (2019) 032707.
[35] COMSOL, RF Module User's Guide, COMSOL, Burlington, MA, 2012.
[36] J.M. Musser, Modeling of heat transfer and reactive chemistry for particles in gas-solid flow utilizing continuum-discrete methodology (CDM) (Doctoral dissertation, West Virginia University Libraries) (2011).
[37] R.W. O'Brien, Thermal or electrical conduction through a granular material, Proc. R. Soc. Lond. A 355 (1682) (1977) 313–333.
[38] R. Prasher, Predicting the thermal resistance of nanosized constrictions, Nano Lett. 5 (11) (2005) 2155–2159.
[39] D. Singh, J.Y. Murthy, T.S. Fisher, Phonon transport across mesoscopic constrictions, J. Heat Transf. 133 (4) (2011).
[40] P. Keblinski, R. Prasher, J. Eapen, Thermal conductance of nanofluids: is the controversy over? J. Nanopart. Res, 10 (7) (2008) 1089–1097.
[41] N. Roy, A. Yuksel, M. Cullinan, Design and modeling of a microscale selective laser sintering system, ASME 2016 11th International Manufacturing Science and Engineering Conference, American Society of Mechanical Engineers Digital Collection, 2016.
[42] N.K. Roy, O.G. Dibua, W. Jou, F. He, J. Jeong, Y. Wang, M.A. Cullinan, A comprehensive study of the sintering of copper nanoparticles using femtosecond, nanosecond, and continuous wave lasers, J. Micro Nano-Manufact. 6 (1) (2018) 010903.
[43] ... D.G. Cahill, W.K. Ford, K.E. Goodson, G.D. Mahan, A. Majumdar, H.J. Maris, S.R. Phillpot, Nanoscale thermal transport, J. Appl. Phys. 93 (2) (2003) 793–818.
[44] D. Rong, M. Horio, DEM simulation of char combustion in a fluidized bed, in: Second International Conference on CFD in the Minerals and Process Industries CSIRO, Melbourne, Australia, 1999, pp. 65–70.
[45] G. Weidenfeld, Y. Weiss, H. Kalman, A theoretical model for effective thermal conductivity (ETC) of particulate beds under compression, Granular Matter 6 (2–3) (2004) 121–129.
[46] A. Yuksel, T.Y. Edward, M. Cullinan, J. Murthy, Uncertainty analysis of near-field thermal energy transfer within nanoparticle packing., in: 2018 17th IEEE Intersociety Conference on Thermal and Thermomechanical Phenomena in Electronic Systems (ITherm), IEEE, 2018, pp. 46–50.
[47] A. Yuksel, E.T. Yu, M. Cullinan, J. Murthy, Heat transfer modeling of nanoparticle packings on a substrate, ASME 2018 International Mechanical Engineering Congress and Exposition, American Society of Mechanical Engineers Digital Collection, 2018.
[48] G.E. Jonsson, V. Miljkovic, A. Dmitriev, Nanoplasmon-enabled macroscopic thermal management, Sci. Rep. 4 (2014) 5111.
[49] M. Fedoruk, M. Meixner, S. Carretero-Palacios, T. Lohmüller, J. Feldmann, Nanolithography by plasmonic heating and optical manipulation of gold nanoparticles, ACS Nano 7 (9) (2013) 7648–7653.